Periodic plasmonic enhancing epitopes on a whispering gallery mode biosensor

Stephen Arnold,[1,2,*] Venkata Ramanaiah Dantham,[1] Curtis Barbre,[1] Bruce A. Garetz,[2] and Xudong Fan[3]

[1]*MicroParticle PhotoPhysics Lab, Department of Applied Physics, Polytechnic Institute of NYU, Brooklyn, New York 11201, USA*

[2] *Department of Chemical and Biomolecular Engineering, Polytechnic Institute of NYU, Brooklyn, New York 11201, USA*

[3]*Department of Biomedical Engineering, University of Michigan, 1101 Beal Ave. Ann Arbor, Michigan 48109,USA*

**SArnold935@aol.com*

Abstract: We propose the attachment of a periodic array of gold nanoparticles (epitopes) to the equator of a Whispering Gallery Mode Biosensor for the purpose of plasmonically enhancing nanoparticle sensing in a self-referencing manner while increasing the capture rate of analyte to antibodies attached to these plasmonic epitopes. Our approach can be applied to a variety of whispering gallery mode resonators from silicon/silica rings and disks to capillaries. The interpretation of the signals is particularly simple since the optical phase difference between the epitopes is designed to be an integer multiple of π, allowing the wavelength shift from each binding event to add independently.

OCIS codes: (280.1415) Biological sensing and sensors; (260.5740) Resonance; (240.6680) Surface plasmons; (230.5750) Resonators; (140.3945) Microcavities

References and links

1. M. S. Luchansky and R. C. Bailey, "High-Q Optical Sensors for Chemical and Biological Analysis," Anal. Chem. **84**(2), 793–821 (2012).
2. Y. Sun and X. Fan, "Optical ring resonators for biochemical and chemical sensing," Anal. Bioanal. Chem. **399**(1), 205–211 (2011).
3. S. Arnold, M. Khoshsima, I. Teraoka, S. Holler, and F. Vollmer, "Shift of whispering-gallery modes in microspheres by protein adsorption," Opt. Lett. **28**(4), 272–274 (2003).
4. F. Vollmer, S. Arnold, and D. Keng, "Single virus detection from the reactive shift of a whispering-gallery mode," Proc. Natl. Acad. Sci. U.S.A. **105**(52), 20701–20704 (2008).
5. S. Arnold, R. Ramjit, D. Keng, V. Kolchenko, and I. Teraoka, "MicroParticle PhotoPhysics illuminates viral biosensing," Faraday Discuss. **137**, 65–83 (2007) (discussion pp. 99–113).
6. V. R. Dantham, S. Holler, V. Kolchenko, Z. Wan, and S. Arnold, "Taking whispering gallery-mode single virus detection and sizing to the limit," Appl. Phys. Lett. **101**(4), 043704 (2012).
7. S. I. Shopova, R. Rajmangal, S. Holler, and S. Arnold, "Plasmonic enhancement of a whispering-gallery-mode biosensor for single nanoparticle detection," Appl. Phys. Lett. **98**(24), 243104 (2011).
8. M. A. Santiago-Cordoba, S. V. Boriskina, F. Vollmer, and M. C. Demirel, "Nanoparticle-based protein detection by optical shift of a resonant microcavity," Appl. Phys. Lett. **99**(7), 073701 (2011).
9. L. Novotny, R. X. Bian, and X. S. Xie, "Theory of nanometric optical tweezers," Phys. Rev. Lett. **79**(4), 645–648 (1997).
10. S. Arnold, D. Keng, S. I. Shopova, S. Holler, W. Zurawsky, and F. Vollmer, "Whispering Gallery Mode Carousel- a photonic mechanism for enhanced nanoparticle detection in biosensing," Opt. Express **17**(8), 6230–6238 (2009).
11. J. Zhu, Ş. K. Ozdemir, Y. F. Xiao, L. Li, L. He, D. R. Chen, and L. Yang, "On-chip single nanoparticle detection and sizing by mode splitting in an ultrahigh-Q microresonator," Nat. Photonics **4**(1), 46–49 (2010).
12. W. Kim, Ş. K. Ozdemir, J. Zhu, L. He, and L. Yang, "Demonstration of mode splitting in an optical microcavity in aqueous environment," Appl. Phys. Lett. **97**(7), 071111 (2010).
13. R. D. Averitt, S. L. Westcott, and N. J. Halas, "Linear optical properties of gold nanoshells," J. Opt. Soc. Am. B **16**(10), 1824–1832 (1999).
14. J. D. Swaim, J. Knittel, and W. P. Bowen, "Detection limits in whispering gallery biosensors with plasmonic enhancement," Appl. Phys. Lett. **99**(24), 243109 (2011).

15. P. Zijlstra, P. M. R. Paulo, and M. Orrit, "Optical detection of single non-absorbing molecules using the surface plasmon resonance of a gold nanorod," Nat. Nanotechnol. **7**(6), 379–382 (2012).
16. W. Ahn, S. V. Boriskina, Y. Hong, and B. M. Reinhard, "Photonic-plasmonic mode coupling in on-chip integrated optoplasmonic molecules," ACS Nano **6**(1), 951–960 (2012).
17. M. Chamanzar and A. Adibi, "Hybrid nanoplasmonic-photonic resonators for efficient coupling of light to single plasmonic nanoresonators," Opt. Express **19**(22), 22292–22304 (2011).
18. M. Chamanzar, E. S. Hosseini, S. Yegnanarayanan, and A. Adibi, "Hybrid Plasmonic-photonic Resonators for Sensing and Spectroscopy," CLEO/QELS San Francisco, CA. 2011, Paper QTuE4.
19. I. M. White, J. Gohring, and X. Fan, "SERS-based detection in an optofluidic ring resonator platform," Opt. Express **15**(25), 17433–17442 (2007).
20. D. Sarid and W. Challener, *Modern introduction to surface plasmons: Theory of Mathematica modeling, and applications* (Cambridge University Press, 2010), Chap. 9.
21. E. S. C. Ching, P. T. Leung, and K. Young, "The role of quasinormal modes," in *Optical Processes In Microcavities*, R. K. Chang, A. J. Campillo, eds. (World Scientific, 1996), pp. 1–75.
22. S. Arnold, "Microspheres, photonic atoms, and the physics of nothing," Am. Sci. **89**, 414–421 (2001).
23. I. Teraoka and S. Arnold, "Resonance shifts of counterpropagating whispering-gallery modes: degenerate perturbation theory and application to resonator sensors with axial symmetry," J. Opt. Soc. Am. B **26**(7), 1321–1329 (2009).
24. A. Mazzei, S. Götzinger, L. S. Menezes, G. Zumofen, O. Benson, and V. Sandoghdar, "Controlled Coupling of Counterpropagating Whispering-Gallery Modes by a Single Rayleigh Scatterer: A Classical Problem in a Quantum Optical Light," Phys. Rev. Lett. **99**(17), 173603 (2007).
25. J. Zhu, Ş. K. Özdemir, L. He, and L. Yang, "Controlled manipulation of mode splitting in an optical microcavity by two Rayleigh scatterers," Opt. Express **18**(23), 23535–23543 (2010).
26. L. Chantada, N. I. Nikolaev, A. L. Ivanov, P. Borri, and W. Langbein, "Optical resonances in microcylinders: response to perturbations for biosensing," J. Opt. Soc. Am. B **25**(8), 1312–1321 (2008).
27. W. Kim, Ş. K. Özdemir, J. Zhu, and L. Yang, "Observation and characterization of mode splitting in microsphere resonators in aquatic environment," Appl. Phys. Lett. **98**(14), 141106 (2011).
28. E. S. Hosseini, S. Yegnanarayanan, M. Soltani, and A. Adibi, "Ultra-high quality factor microdisk resonators for chip-scale visible integrated photonics," in *Frontiers in Optics* (2008), p. FMG4.
29. A. Gondarenko, J. S. Levy, and M. Lipson, "High confinement micron-scale silicon nitride high Q ring resonator," Opt. Express **17**(14), 11366–11370 (2009).
30. M.-C. Tien, J. F. Bauters, M. J. R. Heck, D. T. Spencer, D. J. Blumenthal, and J. E. Bowers, "Ultra-high quality factor planar Si_3N_4 ring resonators on Si substrates," Opt. Express **19**(14), 13551–13556 (2011).

1. Introduction

The label-free detection of individual aqueous borne bio-nanoparticles (*e.g.*, virus, protein) is an important goal in the bio-sensing field; analytes are detected at the ultimate sensitivity, in their native state (*i.e.*, without interference from labels), without added preparation, and size/mass information can be extracted from the signals [1,2]. The first label-free single bio-nanoparticle detection by a microcavity was of InfluenzaA with a mass of 512 attograms (ag) from the reactive frequency shift [3] of a micro-spheroidal Whispering Gallery Mode (WGM) [4]. In reactive sensing the evanescent field of the WGM polarizes the analyte, and as a reaction the cavity's resonance shifts [3]. The limit of detection (LOD) in the InfluenzaA experiment based on the reported signal/noise ratio (S/N) was ~170 ag. Since the reactive frequency shift is in proportion to mass, a virus such as Polio with a mass of 14 ag would not have been detected [5]. Recently, the robust detection (S/N = 8) and sizing of a virus MS2 (6ag), which has less than half the mass of Polio was demonstrated by adding a nanoplasmonic structure ("plasmonic epitope") to the sensing region, thereby forming a Whispering Gallery Mode Hybrid resonator (WGM-h) [6]. This simple addition provided a frequency shift boost ~70x, and brought the LOD down to 0.4 ag (molecular weight equivalent of 240 kDa). This frequency shift enhancement occurs because the WGM drives the plasmonic epitope into resonance, thereby creating local hot spots that increase the reactive interaction between the virus and the cavity [7,8]. In addition, the virus is drawn to the plasmonic receptor due to enhanced light forces [6,7,9,10]. With this simple modification to the microcavity, viruses of all known sizes can be detected one at a time. This achievement means that a virus such as Polio can be detected with the ultimate sensitivity. In addition, the potential applications go well beyond virus to single protein. By projecting from the MS2 experiments, the authors of Ref.6 calculate that protein above an effective radius of 2 nm

(molecular weight ~26 kDa) should be able to be detected and sized. However, an important problem still remains: a single nanoplasmonic epitope has little surface for analyte binding compared to the entire equator of the WGM microcavity. As a consequence, statistics are limited and the time between binding events is long. This paper is concerned with a cure for these problems.

In what follows we propose to attach a necklace of periodic plasmonic epitopes to the surface of a WGM microcavity (*e.g.*, oblate spheroid in Fig. 1), thereby substantially increasing the available surface for analyte binding while still retaining the frequency shift boost. Beyond increasing the number of possible events and reducing the time between events the periodic configuration changes our measurement approach from "spectral step-sensing" [4] to "self-referencing" [11]. Self-referencing can be understood in the following way. On a bare cavity a WGM circulating in a given direction or in the opposite direction will have the same frequency. A particle on the equator couples these modes and splits this degeneracy into two resonances. This splitting is apparent when the reactive shift exceeds the modal linewidth. For a single nanoparticle the splitting is twice the average shift, which enables the interaction to be measured from the frequency separation between the split modes. A large number of periodic epitopes are assured to produce mode splitting even if one epitope does not [12]. The advantage of the "self-referencing" approach to measurement is that it is differential and can therefore eliminate common mode noise. A key advantage of the periodic epitopes is that this design builds a quasi-1D photonic band structure. Near the band edge where the inter-epitope optical phase difference is π, adsorption on any of the plasmonic epitopes produces additional splitting that is simply additive. In what follows we will discuss the enhancement by possible local plasmonic epitopes. Following this we will describe our theoretical approach, apply it to nonperiodic mode splitting problems in the past, and finally to periodic plasmonic epitope sensing of dielectric bio-nanoparticles.

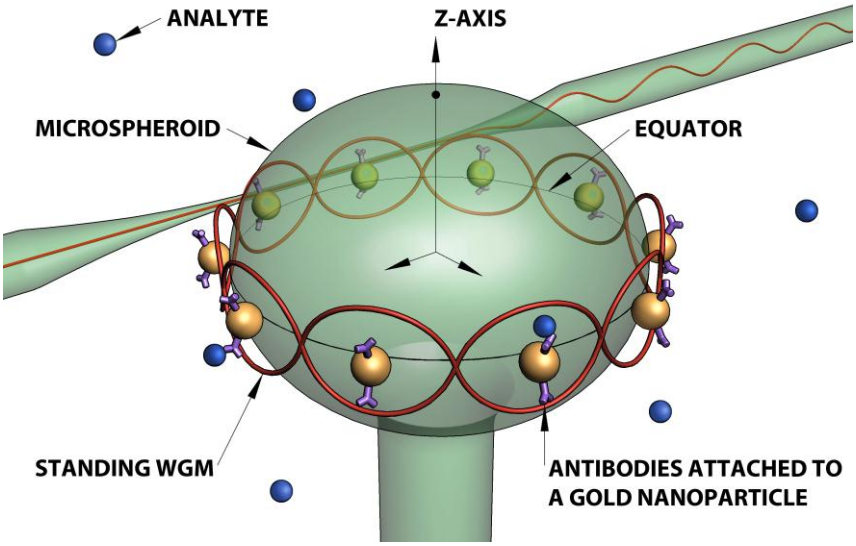

Fig. 1. Illustration of an oblate spheroidal whispering gallery mode (WGM) resonator with functionalized periodic nano-plasmonic epitopes, that is driven at a frequency that produces a symmetric standing wave.

2. Possible plasmonic epitopes

The space group of the 1D structure with its band edge inter-optical phase difference of π is apparent in Fig. 1, however the point group can be picked from a variety of local plasmonic structures. Solid gold spherical particles are a poor choice since they have a modest intensity

enhancement at their hot spots of only ~37x [7], whereas a core shell structure can develop a tenfold further enhancement as shown from the results of quasi-static calculations [13] in Fig. 2(a) [6]. The intensity enhancements in this figure were calculated at the top (T) or bottom (B) of the depicted shell and show the tunability of the core-shell structure as the shell thickness is changed. As in most local plasmonic structures, the field enhancements increase as one moves from the center of the visible spectrum toward the near infrared due to the reduced imaginary component of gold's permitivity in this region [7]. There are also nanoellipsoids [Fig. 2(b)] and nanorods [14,15] that can develop much larger enhancements, but will have to be carefully oriented; for TE excitation the orientation would be along a meridian with hotspots above and below the equator. This is experimentally possible by using micro/nanofabrication methods (such as photolithography and shadow masking, *etc.*) [16–19]. Specific detection can be achieved by functionalizing each epitope's hot spot regions, *i.e.*, with antibodies that exclusively allow binding of distinctive target analytes suspended in aqueous media.

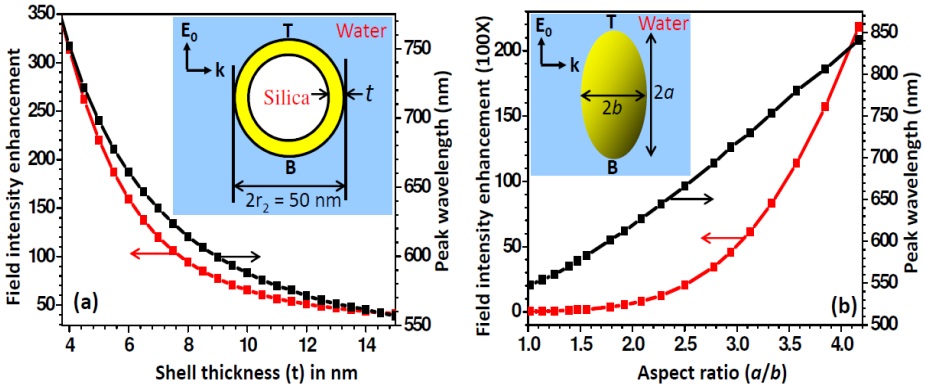

Fig. 2. (a) Maximum electric field intensity enhancement at T or B, and the corresponding peak wavelength location of the dipole mode of a gold nanoshell 50 nm in diameter having a thickness ranging from 3.5 to 15 nm (inset). Note that the wavelength shift for an infinitesimally small bio-particle binding at T or B on a nanoshell grows by a factor of ~340. (b) Maximum field intensity enhancement at the tip (T or B) and the corresponding peak wavelength location of the plasmon mode of a gold ellipsoidal nanoparticle having an aspect ratio ranging from 1.0 to 4.2, calculated using quasi-static approximation [20]. Here 2*b* is 25 nanometers.

3. Theory of one, two and N plasmonic epitopes

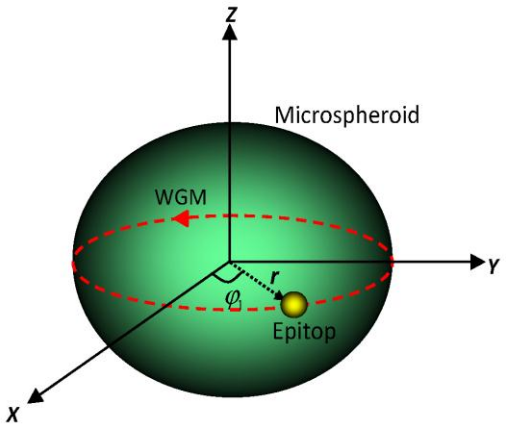

Fig. 3. Illustration of a WGM ring resonator with one epitope.

We start our analysis with a single plasmonic epitope on the equator of a microspheroid (Fig. 3) in an attempt to verify the results of Zhu *et al.* [11] before moving on to the necklace. We concentrate theoretically on the equatorial mode of an oblate axisymmetric microcavity. Without the plasmonic epitope or significant roughness we have a bare cavity in which two counterpropagating equatorial WGMs have identical resonance frequencies; they are degenerate. Since the microcavity is a high *Q* system, the modes of this system can be considered to be quasi-normal modes [21]. This allows for quantum analogs such as photonic atoms [22]. Such analogs compel one to borrow the theoretical machinery of quantum mechanics in order to describe high *Q* optical systems. For bound nanoplasmonic epitope perturbing a WGM, degenerate perturbation theory can be used to predict the eigenvalues and eigenstates of the system.

The oblateness of the spheroid lifts the $2\ell+1$ degeneracy of a sphere allowing the equitorial mode having a principle quantum number *s*, angular momentum quantum number ℓ, and a two fold degeneracy $m=\pm\ell$ to be excited through guided wave excitation. This equitorial WGM (Fig. 3) provides the simplest model for which a first order perturbation will not couple radial modes having different principle quantum numbers since their frequencies do not cross. First, we start to interpret the signal in the presence of a plasmonic epitope attached to the WGM ring (equator) at an angle φ_1, as shown in Fig. 3; then we apply this theory to two epitopes and N epitopes, respectively. The N epitopes will first be considered as random and then periodic.

Our theory will apply the approach of Teraoka and Arnold [23]. We will briefly review the results of this paper before applying it to the case of periodic epitopes.

First we start with the bare cavity framework. By separating the Helmholtz equation the azimuthal differential equation for the equitorial TE mode, which is almost entirely polarized along the polar direction (θ) has the form:

$$\frac{1}{r^2}\frac{\partial^2 E_\theta}{\partial\varphi^2}+k^2E_\theta=0, \tag{1}$$

where *r* is radial variable (~radius of the ring), *k* is the wave vector and E_θ is the electric field. The solutions of the above Eq. take the form

$$E_\theta \sim e^{\pm i\,k\,r\,\varphi}. \tag{2}$$

The orbital boundary condition,

$$E_\theta(\varphi+2\pi m)=E_\theta(\varphi), \tag{3}$$

where integer *m* guarantees that *m* = *kr*. Bare WGM microcavities typically support both clockwise (*cw*) and counterclockwise (*ccw*) equitorial modes, which for the same *m* are degenerate in frequency. Using Eqs. (2) and (3), orthogonal basis vectors for these *ccw* and *cw* equatorial traveling waves are

$$\left.\begin{aligned} |ccw> &= \frac{E^1{}_\theta(r,\theta)}{2}e^{im\varphi}, \\ &\text{and} \\ |cw> &= \frac{E^1{}_\theta(r,\theta)^*}{2}e^{-im\varphi}, \end{aligned}\right\} \tag{4}$$

respectively, where $E^1{}_\theta(r,\theta)$ is the semi-classical field amplitude associated with a single photon. Since our interest is in the TE equatorial mode, $E_\theta^{1*}=-E_\theta^1$ [23]. The dielectric

function of the cavity is $\varepsilon(\boldsymbol{r})$ and consequently the energy in either travelling wave $\hbar\omega = 2 < ccw \mid \varepsilon(\boldsymbol{r}) \mid ccw > = 2 < cw \mid \varepsilon(\boldsymbol{r}) \mid cw >$, where the 2 accounts for an equal amount of electric and magnetic energy in the cavity, the matrix element requires integration over the cavity volume, and the usual conjugate relationship between the bra and ket is maintained. In order to return to a familiar result we will at first suppose that a perturbation to the cavity maintains the travelling wave. Having to polarize an added Rayleigh particle on the equator at position $\boldsymbol{r}_1 = (r_1, \pi/2, \varphi_1)$ with excess polarizability having a real part α_{ex} corresponds to a dielectric perturbation $\alpha_{ex}\,\delta(\boldsymbol{r} - \boldsymbol{r}_1)$. This perturbation costs the cavity energy $\hbar\delta\omega = - < ccw \mid \alpha_{ex}\,\delta(\boldsymbol{r} - \boldsymbol{r}_1) \mid ccw >$ [3], for which the frequency shift of either travelling wave is

$$\delta\omega \approx -\frac{< ccw \mid \alpha_{ex}\,\delta(\boldsymbol{r} - \boldsymbol{r}_1) \mid ccw >}{\hbar}. \tag{5}$$

After the original presentation of Eq. (5) [3], this first order perturbation in frequency of either of the traveling wave states has become known in the literature as *g* [11,24]. Equation (5) is in a conveniently simple form by keeping Planck's constant in place. However, because of our single photon approach $\hbar$ is simply a place saver for the energy in the cavity divided by frequency. With $\hbar$ converted in this way Eq. (5) can be evaluated using our basis states in Eq. (4) and the position $\boldsymbol{r}_1 = (r_1, \pi/2, \varphi_1)$ of the plasmonic epitope with the result [3]:

$$\delta\omega = g = -\frac{\alpha_{ex}\left|\boldsymbol{E}^1{}_\theta(r_1, \pi/2)\right|^2}{2\int \varepsilon(\boldsymbol{r})\left|\boldsymbol{E}^1{}_\theta(\boldsymbol{r})\right|^2 dV}\;\omega. \tag{6}$$

It is important to understand that had we constructed our theory for N_p photons *g* would not change since the intensities in the numerator and denominator scale together with N_p. In what follows we will stick with the form in Eq. (5) by including $\hbar$. However, our description currently is not complete since the dielectric perturbation can couple the traveling wave states.

Coupling requires interaction between the *ccw* and *cw* states through degenerate perturbation theory. For a two state system one has to solve an eigenvalue equation involving a 2x2 matrix

$$-\begin{pmatrix} < ccw \mid \alpha_{ex}\,\delta(\boldsymbol{r} - \boldsymbol{r}_1) \mid ccw > & < ccw \mid \alpha_{ex}\,\delta(\boldsymbol{r} - \boldsymbol{r}_1) \mid cw > \\ < cw \mid \alpha_{ex}\,\delta(\boldsymbol{r} - \boldsymbol{r}_1) \mid ccw > & < cw \mid \alpha_{ex}\,\delta(\boldsymbol{r} - \boldsymbol{r}_1) \mid cw > \end{pmatrix}\begin{pmatrix} a_{ccw} \\ a_{cw} \end{pmatrix} = \hbar\,\delta\omega \begin{pmatrix} a_{ccw} \\ a_{cw} \end{pmatrix}, \tag{7}$$

where a_{ccw} and a_{cw} are amplitudes for being in a superposition state

$$\mid \nu > = a_{ccw} \mid ccw > + a_{cw} \mid cw > . \tag{8}$$

In the absence of an off-diagonal term we return to Eq. (5) as expected. Unique solutions are guaranteed by setting the determinant of the secular equations represented by Eq. (7) equal to zero.

$$\begin{vmatrix} -\dfrac{< ccw \mid \alpha_{ex}\,\delta(\boldsymbol{r} - \boldsymbol{r}_1) \mid ccw >}{\hbar} - \delta\omega & -\dfrac{< ccw \mid \alpha_{ex}\,\delta(\boldsymbol{r} - \boldsymbol{r}_1) \mid cw >}{\hbar} \\ -\dfrac{< cw \mid \alpha_{ex}\,\delta(\boldsymbol{r} - \boldsymbol{r}_1) \mid ccw >}{\hbar} & -\dfrac{< cw \mid \alpha_{ex}\,\delta(\boldsymbol{r} - \boldsymbol{r}_1) \mid cw >}{\hbar} - \delta\omega \end{vmatrix} = 0. \tag{9}$$

The diagonal terms can be written as $g-\delta\omega$, whereas the off-diagonal terms are quickly evaluated from Eqs. (4) since $|cw>=-|ccw>e^{-i\,2m\varphi}$ and consequently the upper rt. element is $-g\,e^{-i\,2m\varphi_1}$, since the perturbation is at azimuthal angle φ_1. The matrix element on the lower left is just the conjugate of this, $-g\,e^{\,i\,2m\varphi_1}$. With these inputs Eq. (9) becomes

$$\begin{vmatrix} g-\delta\omega & -g\,e^{-i\,2\Phi_1} \\ -g\,e^{+i\,2\Phi_1} & g-\delta\omega \end{vmatrix} = 0, \tag{10}$$

where $\Phi_1 = m\varphi_1$ is the optical phase at the epitope. The eigenvalues obtained from the determinant are

$$\delta\omega_{\pm} = g \mp g \quad (i.e.\ \delta\omega_{+} = 0,\ \delta\omega_{-} = 2g), \tag{11}$$

in agreement with Zhu *et al*. [11]. The epitope clearly splits the degeneracy, and the magnitude of the splitting 2|*g*| depends only on the value of *g*. If *g* is a negative number, as it would be for an epitope having a polarizability which is positive, $\delta\omega_{+}$ is larger than $\delta\omega_{-}$. As we go forward the subscript + on the frequency shift will be assigned to the state maintaining the higher frequency for g < 0 (i.e. $\alpha_{ex} > 0$).

So far we have been assuming quasi-normal modes. Losses can cause the modal line widths to overlap, in which case one expects to measure a shift of a single feature that is the average of frequency shift of the two states. In order to look at the wave function amplitudes of the mixed states (*i.e*., the location of the nodes and anti-nodes in the relation to the epitopes), we need to determine the eigenvectors in Eq. (10). The solution of the following equation provides the required eigenvectors,

$$\begin{pmatrix} g-(\delta\omega)_{\pm} & -g\,e^{-i\,2\Phi_1} \\ -g\,e^{+i\,2\Phi_1} & g-(\delta\omega)_{\pm} \end{pmatrix} \begin{pmatrix} a_{ccw} \\ a_{cw} \end{pmatrix}_{\pm} = 0. \tag{12}$$

For simplicity, the epitope is assumed to be on the *X*-axis (i.e., $\Phi_1 = 0$) then this Eq. is reduced as follows,

$$\begin{pmatrix} g-(\delta\omega)_{\pm} & -g \\ -g & g-(\delta\omega)_{\pm} \end{pmatrix} \begin{pmatrix} a_{ccw} \\ a_{cw} \end{pmatrix}_{\pm} = 0. \tag{13}$$

The eigenvalues remain the same ($i.e.\ \delta\omega_{+} = 0, \delta\omega_{-} = 2g$). The relation between eigenvectors corresponding to the eigenvalues $\delta\omega_{+}$ and $\delta\omega_{-}$, respectively are $a_{ccw} = a_{cw}$ and $a_{ccw} = -a_{cw}$. After inserting these relations in the Eq. (8) (using $E_{\theta}^{1*} = -E_{\theta}^{1}$), and normalizing the eigen vectors to a single photon (*i.e.*, $|a_{ccw}|^2 + |a_{cw}|^2 = 1$), we obtain the following new states.

$$|\nu_{+}\rangle = i\,\frac{E_{\theta}^{1}(r,\theta)}{\sqrt{2}}\sin\Phi, \tag{14}$$

and

$$|\nu_{-}\rangle = \frac{E_{\theta}^{1}(r,\theta)}{\sqrt{2}}\cos\Phi. \tag{15}$$

It is clear that these wave functions are mutually orthogonal. In other words, in the presence of an epitope, the wave functions redistribute themselves in such a way that one standing wave mode $|\nu_- >$ has an antinode at the epitope thereby maximizing the interaction; a symmetric standing wave (SSW), resulting in a frequency shift 2*g*. It should be noted that the amplitude squared of the SSW state is twice that of either travelling wave state consistent with the factor of 2 increase in frequency shift. The other state $|\nu_+ >$ minimizes reactive interaction: an antisymmetric standing wave (ASW), resulting in no shift.

If another epitope is attached to the ring at an angle φ_2, then the eigenvalues in the presence of the two epitopes are derived from the determinant

$$\begin{vmatrix} (g_1 + g_2) - \delta\omega & -(g_1 e^{-i2\Phi_1} + g_2 e^{-i2\Phi_2}) \\ -(g_1 e^{i2\Phi_1} + g_2 e^{i2\Phi_2}) & (g_1 + g_2) - \delta\omega \end{vmatrix} = 0, \qquad (16)$$

where $\Phi_2 = m\varphi_2$ represents the optical phase of the wave at the second epitope. The eigenvalues of the system are

$$\delta\omega_\pm = (g_1 + g_2) \mp \sqrt{g_1^2 + g_2^2 + 2g_1 g_2 \cos 2(\Phi_1 - \Phi_2)}. \qquad (17)$$

The total magnitude of the splitting ($\delta\omega_+ - \delta\omega_-$) in the presence of two epitopes is $2\sqrt{g_1^2 + g_2^2 + 2g_1 g_2 \cos 2(\Phi_1 - \Phi_2)}$. This is consistent with the results in Ref [25] and reveals that splitting magnitude is not only determined by the size, shape, and refraction index of the epitope, but also is strongly dependent on the phase difference between them (*i.e.,* relative positions). If the second epitope is identical to the first epitope ($g_1 = g_2 = g$), then the total magnitude of the splitting is $4|g|\cos(\Phi_1 - \Phi_2)$. This clearly indicates that the mode splitting disappears when the phase difference is π/2, which results from the fact that the two epitopes exert the same influence on each of the two standing wave modes. However, if the phase difference between any consecutive epitopes is π, this gives rise to the maximum splitting 4|g|. In order to get the eigenvectors, for simplicity Φ_1 and Φ_2 are assumed to be 0 and π. The solution of the following equation provides the required eigenvectors;

$$\begin{pmatrix} 2g - (\delta\omega)_\pm & -2g \\ -2g & 2g - (\delta\omega)_\pm \end{pmatrix} \begin{pmatrix} a_{ccw} \\ a_{cw} \end{pmatrix}_\pm = 0. \qquad (18)$$

The relation between eigenvectors corresponding to the eigenvalues $\delta\omega_+ = 0$ and $\delta\omega_- = 4g$, respectively are $a_{ccw} = a_{cw}$ and $a_{ccw} = -a_{cw}$. By substituting these relations in the Eq. (8), we get the same mutually orthogonal wave functions given by Eqs. (14) and 15.

Suppose now that N epitopes are attached to the surface in random positions on the ring. Then the eigenvalues of the system are derived from the determinant

$$\begin{vmatrix} (Ng - \delta\omega) & -g\sum_{j=1}^{N} e^{-i\Phi_j} \\ -g\sum_{k=1}^{N} e^{+i\Phi_k} & (Ng - \delta\omega) \end{vmatrix} = 0. \qquad (19)$$

This equation can be written as

$$\left(Ng-\delta\omega\right)^2-g^2\left(N+\sum_{\substack{j,k\\ j\neq k}}e^{i\left(\Phi_k-\Phi_j\right)}\right)=0. \tag{20}$$

For random adsorption the ensemble average $\left\langle \sum_{\substack{j,k\\ j\neq k}} e^{i\left(\Phi_k-\Phi_j\right)} \right\rangle \cong 0.$

Therefore the eigenvalues of the system are $\delta\omega_{\pm}=Ng\mp g\sqrt{N}$ and the magnitude of splitting is $2|g|\sqrt{N}$. This is consistent with the results of Chantada *et al*. [26].

Having shown that our theoretical approach is consistent with the results of others we now apply it to the case of periodic epitopes. If N identical epitopes are periodically attached to the ring in the presence of an optical phase difference ΔΦ between the consecutive epitopes, then the eigenvalues of the system are given by the following equation,

$$\begin{vmatrix}(Ng-\delta\omega) & M_{12}\\ M_{12}^{*} & (Ng-\delta\omega)\end{vmatrix}=0, \tag{21}$$

where $M_{12}=-ge^{-i\,2\Phi_1}\left[1+e^{-i\,2\Delta\Phi}+e^{-i\,4\Delta\Phi}+.....+e^{-i\,2(N-2)\Delta\Phi}+e^{-i\,2(N-1)\Delta\Phi}\right]$. The eigenvalues of this system are

$$\delta\omega_{\pm}=Ng\mp\left|M_{12}\right|=Ng\mp g\left|\frac{\sin(N\,\Delta\Phi)}{\sin(\Delta\Phi)}\right|, \tag{22}$$

When $\Delta\Phi=\pi$ the eigenvalues are

$$\delta\omega_{\pm}=Ng\mp Ng \quad (i.e.\ \delta\omega_{+}=0,\ \delta\omega_{-}=2Ng) \tag{23}$$

The total magnitude of the splitting in this case is 2N|*g*|. This means, when the optical phase difference between consecutive epitopes is π, then frequency shift due to each epitope adds independently. In the presence of 10 epitopes, variation in the frequency shift as a function of ΔΦ is shown in Fig. 4. It can be seen that maximum frequency shift is 20g at ΔΦ = π due to the superposition of the travelling waves, and the average shift for all possible phase differences is 10g; this is exactly the shift produced by a travelling wave. The peak that appears at π is known as the first order peak and higher order peaks appear at integer multiples of π. The peak width is inversely proportional to *N*; in order to observe a significant splitting experimentally, the inter-epitopes phase difference must have an error of less than half of the peak width. If the position of each epitope is Gaussian-distributed around the correct position with standard deviation σ, the mode splitting will be reduced. For example, for an operating wavelength of 800 nm in silica, if σ/r = 0.025 μm/40 μm, the mode splitting becomes 90% of the full splitting. For a smaller σ of 0.015 μm, the fraction rises to 96%. If one epitope is missing, then the model fails. In practice, both issues can be dealt with by quality control and post-fabrication examination. We can also view the proposed periodic epitope system as a diffraction grating, with each epitope being the grating groove. It is well known that the grating sensitivity (resolution) depends upon the total number of grooves illuminated on the surface of the grating (*N*) and diffraction order (*n*). Although the sensitivity (magnitude of splitting) of the proposed epitope system is dependent on *N* like a diffraction grating, it is independent of *n*. In other words, the magnitude of the splitting is the same for all orders.

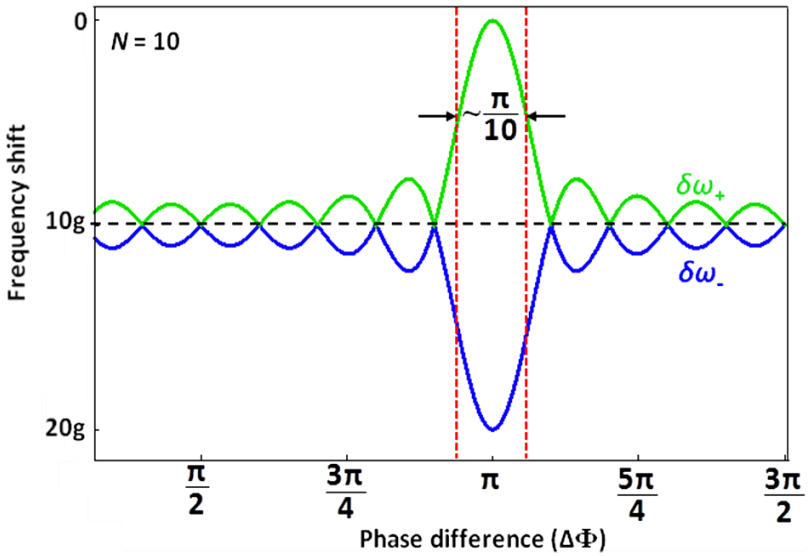

Fig. 4. Variation of the frequency shift of the WGM in the presence of 10 epitopes adsorbed on a microcavity as a function of phase difference between the consecutive epitopes.

The eigenvectors for the *N*-periodic epitope system are given by the following Equation by assuming $\Phi_1 = 0$ and $\Delta\Phi = \pi$.

$$\begin{pmatrix} Ng - (\delta\omega)_{\pm} & -Ng \\ -Ng & Ng - (\delta\omega)_{\pm} \end{pmatrix} \begin{pmatrix} a_{ccw} \\ a_{cw} \end{pmatrix}_{\pm} = 0, \tag{24}$$

The relation between eigenvectors corresponding to the eigenvalues $\delta\omega_+ = 0$ and $\delta\omega_- = 2Ng$, respectively are $a_{ccw} = a_{cw}$ and $a_{ccw} = -a_{cw}$, provide the same mutually orthogonal wave functions given by Eqs. (14) and 15. The eigenstates of a system with 10 epitopes on a ring are shown in Fig. 5. It is clear that all epitopes are at anti-nodes (symmetric mode) in one case, resulting in the maximum frequency shift 20g. In the other case, all epitopes are at nodes (asymmetric mode), which results in no shift.

For N periodic epitopes, that are different from each other, then the eigenvalues of the system are given by the following equation,

$$\begin{vmatrix} \sum_{j=1}^{N} g_j - \delta\omega & -e^{-i\,2\Phi_1} \sum_{j=1}^{N} g_j e^{-i\,2(j-1)\Delta\Phi} \\ -e^{i\,2\Phi_1} \sum_{k=1}^{N} g_k e^{i\,2(k-1)\Delta\Phi} & \sum_{j=1}^{N} g_j - \delta\omega \end{vmatrix} = 0, \tag{25}$$

when $\Delta\Phi = \pi$ the eigenvalues of the system are

$$\delta\omega_{\pm} = \langle \sum g_j \rangle \mp \sqrt{\langle \sum g_j \rangle \langle \sum g_k \rangle} = N\langle g \rangle \mp N\langle g \rangle \quad (i.e.\ \delta\omega_+ = 0,\ \delta\omega_- = 2N\langle g \rangle). \tag{26}$$

In the case of mode splitting, along with the physical properties of the epitopes, the quality factor of the microcavity also plays a major role. To observe the mode splitting requires that its magnitude be considerably larger than the line width of WGM resonance. In the case of a cavity containing *N* particles, the observation of mode splitting requires

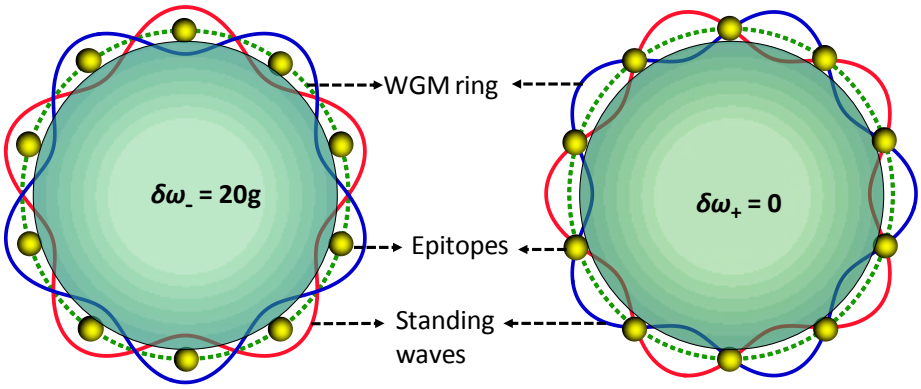

Fig. 5. Two states of a WGM ring with 10 plasmonic epitopes. Here optical phase difference between the consecutive epitopes is π.

$$N\left|2g\right| > N\,\Gamma_e + \Gamma_0 \Rightarrow \left|2g\right| > \Gamma_e + \frac{\Gamma_0}{N}, \tag{27}$$

where Γ_e is the spectral width due to the scattering and absorption losses of an epitope and Γ_0 is the intrinsic resonance width of the bare cavity. Thus, increasing the value of N increases the possibility of observing the splitting.

In single dielectric nanoparticle (*e.g.*, bio-nanoparticle) detection, if a dielectric analyte is adsorbed to any one of the epitopes then (N-1) epitopes have the same interaction with the microcavity (g) and one epitope which adsorbs the analyte particle has the different interaction (g'). Here it is to be noted that g' is the combined interaction of single dielectric analyte particle and epitope with the microcavity. The splitting now changes to $2(N-1)g + 2g'$. Similarly, if two dielectric nanoparticles are adsorbed each at the center of the dipole hot spots of two different epitopes (*i.e.*, position T or B in Fig. 2), then the splitting becomes $2(N-2)g + 4g'$, and so on. Here, the interaction g' is proportional to the real part of effective polarizability $\mathrm{Re}[\alpha_{eff}]$ of a plasmonic-dielectric cluster. Suppose that an extremely small dielectric particle (*i.e.*, a protein molecule) is attached to a spherical plasmonic epitope, then $\mathrm{Re}[\alpha_{eff}]$ for transverse electric (TE) mode excitation can be estimated using the following analytical expression:

$$\mathrm{Re}[\alpha_{eff}] \approx \alpha_{\mathrm{Re}}^{p} + \left|1 + \frac{2\alpha^{p}}{4\pi\varepsilon_0\varepsilon_m a_p^3}\right|^2 \alpha^{d}, \tag{28}$$

where α_{Re}^{p} is the real part of the excess polarizability of the plasmonic epitope, ε_0 and ε_m are the electric permittivities of the vacuum and relative permittivity of the surrounding medium, respectively, a_p is the radius of the plasmonic epitope (*e.g.*, solid gold sphere or gold shell structure as in Fig. 2), α^{d} excess polarizability of the adsorbed dielectric particle, and the squared quantity on the right hand side is the intensity enhancement factor at the center of the hot spot.

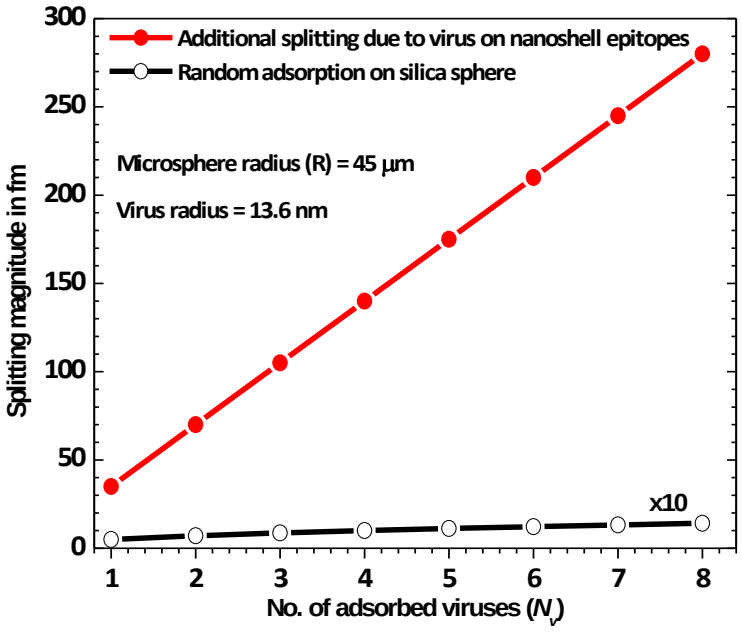

Fig. 6. Comparison between the mode splitting magnitude upon adsorbing 8 randomly located viruses to a bare microsphere equator (black) with the additional splitting for binding the same viruses to periodic plasmonic nanoshell epitopes (N = 4) on a similar microsphere (red).

Figure 6 demonstrates the advantage of the periodic plasmonic epitope system with respect to sensing. We first start the discussion of this figure by considering adsorption onto the equator of a bare resonator (lower trace), and take our analyte to be the smallest aqueous borne RNA virus [MS2, 13.6 nm radius]. This discussion will be an extension of Ref [6] for which the radius of the silica resonator was $45\mu m$ and the unperturbed resonance occurs near a free space wavelength of 780nm [6]. To be consistent with Ref [6], we will talk of shifts, splittings and linewidth changes in wavelength terms. Adsorption on the silica equator is calculated to produce a resonance shift of 0.25 fm, well below the 2fm r.m.s. noise in Ref.6. The calculated splitting would be 2x0.25 = 0.5 fm, much smaller than the experimental linewidth of 1950fm (Q = 4x10^5). If 8 copies of the virus adsorbed randomly on the equator of this resonator the mean splitting for a statistical number of trials would be $2x0.25x\sqrt{8}$ =1.4 fm, still much smaller than the line width. Even if we increase the Q to ~4x10^6 (line width = 195 fm), a value easily within reach of such a microcavity [27], the splitting due to these 8 viruses would still not be seen. It is to be noted that the mode splitting due to the imperfections (Rayleigh scattering) will be present when the ring resonator has an extremely high Q-factor (~10^8). With a low Q-factor, such a splitting does not occur. In our case, because of the lossy metallic nanoparticles, our Q-factor is much lower (~10^6).

Next we consider the effect of including functionalized periodic plasmonic epitopes as binding sites. We suppose now that epitopes are added to the microcavity described in the preceding paragraph. These epitopes will be of the same type as the single epitope used in Ref.6 (gold nanoshell with silica core). We will need some additional experimental information concerning the shift $|g|$ and linewidth change Γ_e produced by the addition of the single nanoshell; in wavelength terms we have measured these to be 175 fm and 230 fm, respectively, during our experiments described in Ref. 6. From the inequality Eq. (27) no splitting would be seen for the adsorption of a single nanoshell for a Q ~4x10^6 ; 2|g| = 350 fm does not exceed the overall linewidth of 425 fm (195 fm from the original linewidth plus 230

fm caused by the deposition of a nanoparticle). Splitting would be seen for two epitopes separated by an optical phase of $n\pi$ since the magnitude of the splitting is 700 fm compared with an overall linewidth of 635 fm. With 4 optimally placed epitopes the splitting magnitude would be 2x4x175 = 1400 fm, well in excess of the overall linewidth. The key question now is: how much additional splitting will be produced by the binding of viruses onto the functionalized hotspots of these epitopes? From Ref.6, which only used one epitope, the maximum shift for a virus was 17 fm, which would have produced an unseen increase in splitting of 34 fm. With 8 viruses adsorbing on our 4 epitopes for which a splitting should be apparent, an increase in splitting of ~280 fm is calculated (upper trace in Fig. 6). So we have gone from an invisible splitting of 3.5 fm by random adsorption on silica to a visible increase of 280 fm for adsorption onto a phased array of 4 epitopes.

4. Discussion

Ultimately the above ideas are envisioned to be used for ring or disk resonators formed by micro and nanofabrication. The use of plasmonic epitopes easily recovers sensitivity lost due to lower Q factors, by providing a boost in signal strength [7]. Such a ring configuration is shown in Fig. 7.

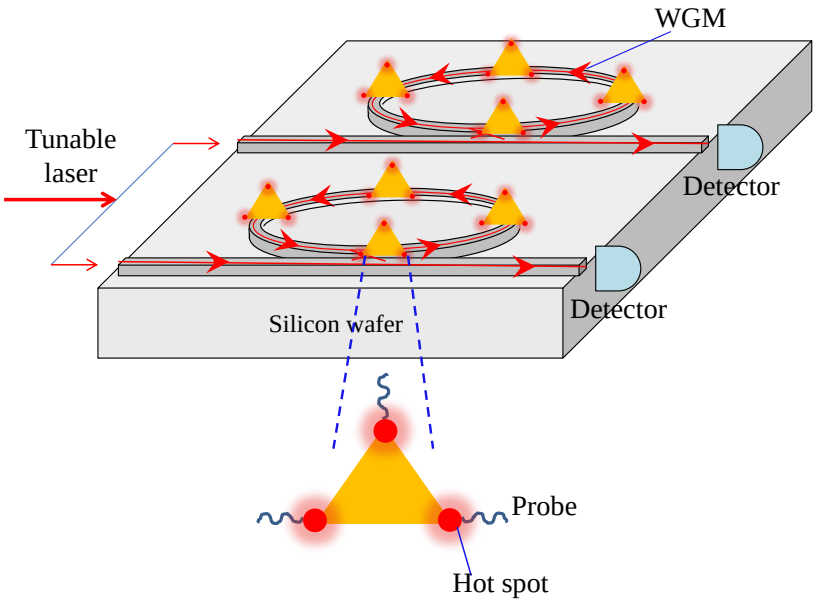

Fig. 7. A multiplexed ring resonator sensor on a chip.

Recent research shows that silicon nitride rings on silicon can provide a Q-factor above 10^6 in the near infrared [28–30], where modes of plasmonic epitopes are easily excited, and single virus and protein detection can be anticipated. By using an array of ring resonators with each carrying different selective receptors, a lab on a chip multiplexed to the same laser can be anticipated.

Acknowledgments

S.A. and B.G. thank the NSF for supporting this work (Grant No. CBET 0933531). X.F. thanks the NSF for supporting this work (Grant No. CBET 1037097 and 1158638).